(ISSI 2021) Path-dependent progressive failure analysis for 3D-printed continuous carbon fibre reinforced composites

Yuan Chen (augustu@163.com)
The University of Sydney https://orcid.org/0000-0001-5651-8560
Lin Ye
Southern Univeristy of Science and Technology

Research Article

Keywords: 3D printing, continuous carbon fibre, modelling, energy absorption, negative Poisson's ratio.

Posted Date: April 4th, 2022

DOI: https://doi.org/10.21203/rs.3.rs-1319267/v1

Abstract

In this study, a novel path-dependent progressive failure (PDPF) numerical approach is developed to predict the damage behaviours of 3D-printed continuous carbon fibre (CCF) reinforced composites when additional short carbon fibre (SCF) composite components are employed for continuous printing or special functionality. First, a progressive failure model using Hashin failure criteria with continuum damage mechanics to account for the damage initiation and evaluation of 3D-printed CCF reinforced polyamide (PA) composites is developed, and an elastic-plastic model is employed to predict the plastic damage behaviours of SCF/PA parts, based on actual fibre placement trajectories with physical measurements of 3D-printed CCF/PA constituents. Then, the accuracy of the PDPF model was validated and utilised to study 3D-printed CCF/PA composites with either negative Poisson's ratio or high stiffness. The results demonstrate that the proposed PDPF model can achieve higher prediction accuracies in mechanical properties of these 3D-printed CCF/PA composites. Mechanism analyses show that the stress distribution is generally aggregated in the CCF areas along the fibre placement paths, and the shear damage and matrix tensile/compressive damage are the key damage modes. This study provides a new approach with valuable information for characterising complex 3D-printed continuous fibre-matrix composites with variable mechanical properties and multiple constituents.

1. Introduction

Fibre reinforced composites and especially continuous carbon fibre (CCF) reinforced composites are well-established as advanced materials with excellent stiffness- and strength-to-weight ratios for a wide range of industrial applications [1, 2]. Conventional manufacturing technologies are sometimes inconvenient, expensive and even incapable of producing CCF composites of extraordinary configurations to satisfy new design purposes and requirements, while 3D printing technology (i.e., additive manufacturing) has become increasingly important and effective to easily achieve new CCF composites with complex configurations and constituents. However, unlike conventionally manufactured CCF composites, as mentioned, usually 3D-printed CCF composites not only have complex structural geometries but also nonuniform fibre paths with variable mechanical properties and multiple constituents, which impedes their effective modelling and analysis for engineering applications.

Currently, research work for modelling 3D-printed CCF composites is limited, though numerical analysis demonstrates strong advantages for investigating structural/material responses and minimising experimental cost. In this context, several recent studies have been attracting researchers' attention to simulations. For instance, Abadi et al. [3] used finite element analysis to characterise the performance of 3D-printed continuous fibre reinforced composites. Majko et al. [4] performed numerical approaches based on the commercial software ADINA to analyse 3D-printed composite laminates reinforced with different fibre categories, i.e., continuous aramid, carbon and glass fibres. Van de Werken et al. [5] developed a numerical model to calculate the damage condition based on Tsai-Wu failure indices of a 3D-printed CCF composite dog bone specimen under tensile loading. Zhang et al. [6, 7] simulated 3D-

printed continuous fibre reinforced composite plates with a central hole when subjected to tension and shearing.

However, numerical modelling of thermoplastic-matrix specimens reinforced with continuous fibres obtained by 3D printing, i.e., fused filament fabrication (FFF), is still in its infancy [8]. Besides, most designed continuous fibre paths are complicated and additional material components are sometimes essential for continuous printing or special functionality of 3D-printed CCF reinforced composites. This has led to variable mechanical properties and multiple constituents [9, 10], while few relevant reports on such modelling methods are available.

In this study, a path-dependent progressive failure (PDPF) approach is proposed to predict and characterise 3D-printed CCF reinforced polyamide (PA) composites, i.e., two topologically-designed CCF composite structures with particular properties: negative Poisson's ratio and high stiffness. In these, short carbon fibre reinforced PA (SCF/PA) components are additional constituents. Numerical models are based on continuum damage mechanics for progressive failure analysis of 3D-printed CCF/PA composites. These are developed by defining the physical fibre placement trajectories as the longitudinal fibre directions within the CCF areas. An elastic-plastic failure model for SCF/PA components based on experimental characterisation is also performed. The prediction results, in terms of the stiffness, peak force and energy absorption of 3D-printed CCF composites, are experimentally and numerically validated.

2. Specimen Preparation And Experiments

Structures with specifical performance can be usually acquired via topological design [11–13]. In this study, the specimens functionalised with either negative Poisson's ratio/auxetic performance or high stiffness were obtained based on topological and fibre placement design using CCFs, as reported in [14]. A Markforged® MII 3D printer was utilised to additively manufacture the CCF/PA functional composites where some areas were printed with SCF/PA (deposited with ±45° configurations, i.e., $+45^{o}$ and -45^{o}, alternatively) for the sake of continuous printing [10]. The final CCF printing trajectories for the specimens with negative Poisson's ratio and high stiffness are shown in Figures 1(a) and (b), respectively. The CCF/PA and SCF/PA filaments for 3D printing were commercially acquired from Markforged Inc. For the 3D-printed composites, the single-layer thickness was 0.125 mm to form 64 layers with a total thickness of 8 mm. The printing paths in each layer are the same as seen in Figures 1(a) or (b), except for the upper and bottom surface layers which were deposited with SCF/PA under a compulsory default setup in Markforged system.

Based on ASTM D638, tensile tests were conducted using an Instron 3366 universal testing machine with a quasi-static constant displacement rate of 5.0 mm/min and a strain gauge with a gauge length of 12.5 mm to measure the effective stress-strain relation of the 3D-printed SCF/PA composite materials (deposited in ±45° configurations).

Compression tests were conducted on the 3D-printed CCF reinforced specimens using an MTS 810 material testing machine with a data acquisition system to record the force-displacement curves. The displacement rate was set at 2.0 mm/min for all the compressive tests, as shown in Figure 1(c). During characterisation, the stiffness and peak force can be directly extracted while the energy absorption can be integrated from the force-displacement curve.

A digital image correlation (DIC) technique was employed to characterise the deformation and mechanical performance of the 3D-printed composites. For the DIC analysis, a white-coloured coating was sprayed on the surface of the planar lattice followed by the application of a uniform pattern of black dots applied using an embossed ink-covered roller. These black dots could be captured by the DIC camera to enable the determination of the displacements or strains. The accuracy of the measured displacement was approximately ±0.02%.

3. A Path-dependent Progressive Failure Analysis

As mentioned before, the complex curvilinear fibre trajectories of 3D-printed continuous fibre composites, such as those shown in Figure 1(a) and (b), lead to variable mechanical properties which are difficult to be accurately modelled using a conventional progressive failure (CPF) model based on approximated fibre orientations with continuum damage mechanics [9, 15]. In this study, a novel numerical modelling method, i.e., a PDPF analysis model, is proposed and developed to predict and analyse the progressive failure response of 3D-printed CCF composites.

First, the actual fibre deposition trajectories are straightforwardly extracted from the Markforged system. Then, the basic width of consolidated CCF/PA filaments is experimentally measured and determined as shown in Figure 2(a), leading to a width value of around 0.72 mm for the 3D-printed CCF/PA in the fibre rich areas. The fibre rich area is where the fibre filaments are deposited back and forth without any gap and within which there are no other material parts.

Taking the CCF composites with negative Poisson's ratio as an example, based on the basic fibre width of 0.72 mm and fibre trajectories of Figure 1(a), the areas of 3D printed CCF/PA parts with their fibre placement directions can be determined as presented in Figure 2(a). Besides, the mechanical properties in the rich area are the same as those of 3D-printed CCF/PA standard tensile specimens that can be experimentally characterised, as reported in [16, 17]. The curved areas of 3D-printed CCF composites may possess a lower fibre volume fraction due to fibre loss during printing [18], however the effect is not considered in the PDPF model due to its marginal impact in this study.

3.1 Progressive failure of 3D-printed CCF/PA composite

The damage behaviours of CCF composites are complicated. They comprise intralaminar damage e.g., continuous fibre fracture/rupture, matrix cracking/crushing and interlaminar damage/delamination. [19].

To date, continuum damage mechanics is of great advantage in calculating the intralaminar damage of CCF composites in a damage accumulation manner based on the damage variables ranging from 0 to 1, for the description of a damage initial state and the progressive development process. In the PDPF model, the orthogonal material constitutive equations were developed based on continuum elements in an Abaqus simulation platform, and the corresponding failure criteria were utilised for calculating the damage initiation and propagation. Among several failure criteria [20–24], one of the mostly utilised method for unidirectional CCF composites, namely, Hashin criterion [21, 22], was employed to predict the failure responses of the 3D-printed CCF composites.

Details for the constitutive equations and failure criteria for 3D-printed CCF/PA composites are presented in Appendix A. The basic mechanical properties were obtained from previous studies [9, 17] for the same 3D-printed CCF/PA composites, with a nominal CCF volume fraction of 31.4% and a void content of 7.5% [17]. With these previous characterisations, the basic mechanical properties are summarised in Table 1. In this study, the interlaminar damage/delamination was observed as an insignificant behaviour [14], hence it has not been taken into account.

As mentioned, in the PDPF model, the 3D-printed CCF/PA filaments in composite layers were calculated using anisotropic material constitutive properties, where the fibre longitudinal direction was defined along the CCF filament trajectories. The fibre transverse direction was then automatically set as perpendicular to the longitudinal direction, as exhibited in Figure 2(a).

Table 1
Mechanical properties of 3D-printed CCF/PA composites [9, 17].

Properties	Variable	Value
Density (kg/m^3)	ρ	1250
Fibre volume (%)	V	31.4
Longitudinal Young's modulus (GPa)	E_{11}	69.4
Transverse Young's modulus (GPa)	E_{22}	3.5
Principal Poisson's ratio (-)	v_{12}	0.33
Shear modulus (GPa)	G_{12}	1.9
Longitudinal tensile strength (MPa)	X_T	905.3
Longitudinal compressive strength (MPa)	X_C	426
Transverse tensile strength (MPa)	Y_T	17.9
Transverse compressive strength (MPa)	Y_C	66
In-plane shear strength (MPa)	S_{12}	43.4
Longitudinal traction fracture energy (KJ/m^2)	G^C_{ft}	91.6
Longitudinal compression fracture energy (KJ/m^2)	G^C_{fc}	79.9
Transverse traction fracture energy (KJ/m^2)	G^C_{mt}	0.22
Transverse compression fracture energy (KJ/m^2)	G^C_{mc}	1.1

3.2 Elastic-plastic behaviour of SCF/PA composite

As previously mentioned, SCF/PA was utilised as additional material components filling the space where CCF/PA placement was difficult in continuous printing. SCF/PA was selected because of its better performance than the PA counterpart [10]. As introduced in Section 2, the SCF/PA filament was placed in ±45° configurations in all printing, and the nominal volume fraction was ~10% [9], leading to an increment of elastic modulus of PA but providing no big improvement in tensile strength. Hence, for modelling purposes, it was treated as an isotropic material for numerical analysis, though it has minor orthotropy [9].

Instead of using the testing results presented in [16], the mechanical properties of 3D-printed SCF/PA composites were specifically characterised in this study. According to ASTM D638, tensile tests were conducted for type IV dog bone SCF/PA specimens (deposited with ±45° path configurations), using a universal testing machine with a quasi-static constant velocity of 5.0 mm/min and a strain gauge with a gauge length of 10 mm to obtain the effective or engineering stress-strain relation.

The mean results of the experimental stress-strain curves of standard specimens produced by repetitive testing were extracted and converted into the true stress-strain curve for modelling [25], as shown in Figure 3. Then, an elastic-plastic model was established using the true stress-strain curve. A summary of its basic properties is depicted: the density is 1160 kg/m^3, tensile modulus is 898 MPa, tensile strength is 50 MPa and failure strain is 0.4. In failure analysis, the equivalent plastic strain (PEEQ) describing an accumulation of the plastic deformation during the process was utilised for characterising the plastic deformation. This was done because of PEEQ's wide applications with benefits for comprehensive and effective evaluation using a scalar rather than a complex strain tensor [26, 27]. In addition, a ductile criterion in Abaqus was applied to determine the final failure of SCF/PA materials using a predefined failure strain (=0.4) based on the elastic-plastic model, to exhibit the materials' fracture behaviour.

3.3 Numerical definitions and boundary conditions

As shown in Figure 2(b), the through-thickness distribution of sixty-two layers of 3D-printed CCF/PA with additional SCF/PA parts and two layers of complete SCF/PA was numerically built, with two SCF/PA layers of the upper and bottom surfaces being compulsory options because of using the Markforged printer. Hence, the specimens consisted of sixty-four plies and each ply had the same thickness of 0.125 mm, based on the printing setup. In each layer, the continuous fibre longitudinal directions, as mentioned, were defined to be the same as those of printing trajectories as shown in Figure 1(a). With the Markforged printer, there is one single wall of SCF/PA, as the casing around a printed profile, which was ignored in the simulation, due to its very limited volume fraction and insignificant effects on characterisation.

The numerical models were developed using Abaqus/Explicit to calculate the structural responses and materials failure. Under compression, 8-node quadrilateral continuum shell elements (SC8R) were applied to guarantee accurate modelling and to improve the calculation's efficiency [2]. The moving and fixed plates were modelled with conventional shell elements (S4R). After a convergence study on mesh and velocity, a constant displacement rate of 100 mm/s was applied for the moving plate and a uniform mesh with the element size of 0.9 mm was used for modelling the 3D-printed specimens [9].

The meshwork of 3D-printed CCF/PA auxetic composite and specific boundary conditions are exhibited in Figure 2(c). A general contact algorithm was deployed to calculate and simulate the general interaction between the elements [25]. The friction coefficients for the contact interfaces were generally defined as 0.3. During the simulation, in accordance with the failure criteria for CCF/PA and the failure strain for SCF/PA, the totally failed elements were removed for further calculation. The same numerical definitions were performed for modelling the high stiffness 3D-printed CCF composites.

4. Results And Discussion

4.1. Case Study 1: auxetic composites

The first case is a 3D-printed auxetic composite with fibre deposition trajectories as shown in Figure 1(a) and subjected to in-plane compression as introduced previously. The experiments show that these CCF/PA composite structures demonstrate a negative Poisson's ratio from −0.2 to −0.1 as the compression displacement progresses from 0 mm to 4 mm within the effective displacement [9] (so the DIC photographic analysis and numerical modelling were performed at 4 mm).

Their force-displacement curves are presented in Figure 4. We can see that the force increases from zero to around 500 N where the surfaces of upper and bottom unit cells were contacted at about 2mm, then the force is further increased to peak at about 2,000 N, and afterwards it gradually decreases when the compressive displacement is over 4 mm. In comparison, the predicted force-displacement curve of the PDPF model agrees well with those of experiments.

The compression behaviours captured for strain analysis by DIC and stress analysis by simulation at Point A of 4 mm are shown in Figure 4. The DIC results demonstrate that both positive and negative horizontal strain ε_{xx} are intersectionally aggregated in the CCF/PA auxetic composites, contributing to their auxetic behaviours. From the stress analysis and CCF trajectories presented in Figure 1(a), it can be seen that Mises stresses are mainly concentrated in the CCF areas along the fibre placement paths, especially in those CCFs against the vertical compression loading, where the maximum stress is 283.9 MPa.

Failure mechanism analyses were performed for 3D-printed CCF/PA auxetic composite with respect to the CCF/PA damage characteristics (Hashin criteria) and SCF/PA plastic deformations (PEEQ) at displacement Point A of 4 mm when under in-plane compression. The results are shown in Figure 5. It is found that fibre damage is not predominant for the 3D-printed CCF/PA auxetics. Shear damage and matrix tensile/compressive damage can be observed at the ligaments within each unit cell, which is attributed to the auxetic behaviours of each unit cell under compression. In terms of the plastic deformation for the SCF/PA parts, slight damage is observed at local contact areas near the moving and fixed plates.

In order to investigate the mechanical performance and model effectiveness for the 3D-printed CCF/PA auxetic composite under in-plane compression, its stiffness, peak force and energy absorption calculated by experiments, PDPF model and CPF model are shown in Figure 6. By experiments, the (mean) stiffness of 3D-printed CCF/PA composite auxetics is 219.7 N/mm, while the predicted results by the PDPF and CPF models are 254.4 N/mm and 289 N/mm, respectively. This indicates that the accuracy using the PDPF model has been improved by 16% as compared to that using the CPF model. The peak forces predicted by PDPF and CPF models are almost at the same level, with a variation of −3.9% and 3.5%, respectively, from the experimental (mean) peak force of 1982.6 N. Finally, the (mean) energy absorption

of 3D-printed CCF/PA auxetic was experimentally measured as 10.6 J, which is 10.8%and 13.4% smaller than those predicted by PDPF and CPF models, respectively. Therefore, the accuracy using the PDPF method has been enhanced by 2.6%. Apparently, the PDPF model is more accurate in the prediction of mechanical performance of 3D-printed auxetic composites.

4.1. Case Study 2: high stiffness composites

The second case is a topologically-designed 3D-printed CCF/PA high stiffness composite with a structural configuration and fibre placement trajectories as shown in Figure 1(b). The basic structural size (80 mm×80 mm×8 mm) and boundary conditions were the same as those of CCF/PA auxetic composites. By experiments and simulation, the compressive force-displacement curves with the compressive responses of 3D-printed CCF/PA high stiffness composites are shown in Figure 7. The force of CCF/PA has a rapid increment to over 12,000 N before the displacement is 2 mm; subsequently, the force decreases steadily to below 6,000 N. In comparison, the force propagation trend is well predicted by the PDPF model. By observation of the compressive behaviours, the local strain concentration can be seen at the contact areas nearing the plates, which is also reflected by the stress distribution in the simulation results. In addition, the stress distribution is generally aggregated in the CCF areas along the fibre placement paths, with the maximum stress reaching 904.7 MPa.

As shown in Figure 8, failure analyses show that the shear damage and matrix tensile/compressive damage are still the key damage mechanisms for CCF/PA parts. However, the damage magnitude of the 3D-printed CCF/PA high stiffness composite is much more severe than that of the CCF/PA auxetic composite. Further, the damage mainly occurred at the four corners and central area, where either fibre shortage or discontinuity generally existed, as indicated by the fibre trajectories shown in Figure 1(b). While the plastic deformation is also basically located around the four corners and the central area, it is locally concentrated with insignificant distributions.

The mechanical performance of 3D-printed CCF/PA high stiffness composites by experiments and simulation are presented in Figure 9. The (mean) stiffness and peak force in experiments are 9301.7 N/mm and 13197.2 N, respectively, which are accordingly around 10% and under 2% of difference to those predicted using either PDPF or CPF model. However, the experimental (mean) energy absorption is 38.5 J, with a variation of 9.5% and 21.6% from those predicted by the PDPF and CPF models, respectively, indicating that the modelling accuracy is improved by 12% when using the PDPF model. The conclusion can be drawn that the PDPF model has higher modelling accuracy than the CPF model for 3D-printed CCF composites.

5. Conclusions

In this study, a novel PDPF analysis approach was developed to predict the progressive failure behaviours of 3D-printed CCF/PA composites with either negative Poisson’s ratio or high stiffness. Key points can be summed up as follows.

When there are additional SCF/PA composite parts, the specific distributions of 3D-printed CCF/PA and SCF/PA components were determined based on actual fibre placement trajectories with physical measurements. Then, a path-dependent progressive failure analysis method using the orthogonal material constitutive relations with continuum damage mechanics based on Hashin failure criteria was developed to account for the damage initiation and evaluation of 3D-printed CCF/PA composites. An elastic-plastic model with a ductile failure method was employed to predict the plastic damage behaviours of SCF/PA composite parts.

Two cases on 3D-printed CCF/PA composites, one with negative Poisson's ratio and the other with high stiffness were calculated for validation and characterisation. The results demonstrated that the PDPF model can well predict not only the force-displacement curves but also the damage behaviours of multiple constituents, i.e., CCF/PA and SCF/PA, in both cases. Besides, as compared to the CPF modelling method, the current PDPF model generally had higher prediction accuracies, such as a 16% and 12% improvement in the prediction of the stiffness of 3D-printed CCF/PA composite auxetics and the energy absorption of 3D-printed CCF/PA high stiffness composites, respectively.

Mechanism analyses showed that the stress distribution was generally aggregated in the CCF areas along the fibre placement paths, and the shear damage and matrix tensile/compressive damage were the key damage mechanisms for both 3D-printed CCF/PA auxetic and high stiffness composites. However, the damage magnitude of the 3D-printed CCF/PA high stiffness composite was much more severe than that of the CCF/PA auxetic composite. In contract, plastic deformation was basically locally concentrated with insignificant distributions.

In this study, we established and proved a new effective modelling method for 3D-printed CCF/PA composites, providing valuable choices and information for predicting complex 3D-printed continuous fibre-matrix composites with variable mechanical properties and multiple constituents.

Declarations

Acknowledgements

The authors appreciate the invitation from Professor Shan-tung Tu and Professor Guoyan Zhou for submission of our research work to the Chinese Journal of Mechanical Engineering.

Authors' Contributions

Yuan Chen performed conceptualisation, formal analysis, and drafting & review & editing, Lin Ye received resources and performed review & supervision.

Authors' Information

Yuan Chen is currently undertaking a Research Fellow position as ARC Postdoctoral Research Associate in the University of Sydney. He obtained his PhD degree from the University of Sydney in 2019. His

research interests are concentrated on additive manufacturing of composite materials, design and computational analysis of composite structures, topological and structural optimisation for metamaterials and advanced composites.

Lin Ye (Fellow of Australian Academy of Technology and Engineering) is currently a Chair Professor at the School of System Design and Intelligent Manufacturing (SDIM) of Southern University of Science and Technology. His research interests include composites science and technology, smart materials & structures, structural integrity and durability, etc.

Funding

The authors acknowledge support from the ARC Discovery Project (DP190102354) and the School of Aerospace, Mechanical and Mechatronic Engineering (AMME), the University of Sydney.

Availability of data and materials

The datasets supporting the conclusions of this article are included within the article.

Competing Interests

The authors declare no competing financial interests.

References

1. Sun Y, Cai Z–B, Wu S–Bo, Liu J–H, Yu J–X. Effect of cycling low velocity impact on mechanical and wear properties of CFRP laminate composites. Chin J Mech Eng 2018; 31:112.
2. Chen Y, Ye L, Fu KK. Progressive failure of CFRP tubes reinforced with composite sandwich panels: Numerical analysis and energy absorption. Compos Struct 2021; 263: 113674.
3. Abadi HA, Thai HT, Paton-Cole V, Patel VI. Elastic properties of 3D-printed fibre-reinforced structures. Compos Struct 2018; 193: 8–18.
4. Majko J, Saga M, Vasko M, Handrik M, Barnik F, Dorčiak F. FEM analysis of long-fibre composite structures created by 3D printing. Transportation Research Procedia 2019; 40: 792–799.
5. Van de Werken N, Hurley J, Khanbolouki P, Sarvestani AN, Tamijani AY, Tehrani M. Design considerations and modeling of fiber reinforced 3D-printed parts. Compos Part B Eng 2019; 160: 684–92.
6. Zhang HQ, Yang DM, Sheng Y. Performance-driven 3D printing of continuous curved carbon fibre reinforced polymer composites: A preliminary numerical study. Compos Part B Eng 2018; 151: 256–64.
7. Zhang HQ, Dickson AN, Sheng Y, McGrail T, Dowling DP, Wang C, Neville A, Yang DM. Failure analysis of 3D-printed woven composite plates with holes under tensile and shear loading. Compos Part B Eng 2020; 186: 107835.

8. Polyzos E, Hemelrijck DV, Pyl L. Numerical modelling of the elastic properties of 3D-printed specimens of thermoplastic matrix reinforced with continuous fibres. Compos Part B Eng 2021; 211: 108671.
9. Chen Y, Ye L, Zhang YX, Fu KK. Compression behaviours of 3D-printed CF/PA metamaterials: Experiment and modelling. Int J Mech Sci 2021; 206: 106634.
10. Chen Y, Ye L. Topological design for 3D-printing of carbon fibre reinforced composite structural parts. Compos Sci Technol 2021; 204: 108644.
11. Zhu BL, Zhang XM, Liu M, Chen Q, Li H. Topological and shape optimization of flexure hinges for designing compliant mechanisms using the level set method. Chin J Mech Eng 2019; 32:13.
12. Gao J, Xiao M, Zhang Y, Gao L. A comprehensive review of isogeometric topology optimization: methods, applications and prospects. Chin J Mech Eng 2020; 33:87.
13. Chen Y, Ye L, Xu C, Zhang YX, Fu KK. Multi-material topology optimisation of micro-composites with reduced stress concentration for optimal functional performance. Mater Design 2021; 210: 110098.
14. Chen Y, Ye L. Designing and tailoring effective elastic modulus and negative Poisson's ratio with continuous carbon fibres using 3D printing. Compos Part A Appl Sci Manuf 2021; 150: 106625.
15. He Y–L, Davim JP, Xue H–Q. 3D progressive damage based aacro–mechanical FE simulation of machining unidirectional FRP composite. Chin J Mech Eng 2018; 31: 51.
16. He Q, Man ZY, Chang L, Ye L. On structure-mechanical and tribological property relationships of additive manufactured continuous carbon fiber/polymer composites. Structure and Properties of Additive Manufactured Polymer Components. Woodhead Publishing, 2020.
17. Iragi M, Pascual-González C, Esnaola A, Lopes CS, Aretxabaleta L. Ply and interlaminar behaviours of 3D-printed continuous carbon fibre reinforced thermoplastic laminates; effects of processing conditions and microstructure. Addit Manuf 2019; 30: 100884.
18. Shiratori H, Todoroki A, Ueda M, Matsuzaki R, Hirano Y. Compressive strength degradation of the curved sections of 3D-printed continuous carbon fiber composite. Compos A Appl Sci Manuf 2021; 142: 106244.
19. Wang X, Tian XY, Lian Q, Li DC. Fiber traction printing: a 3D printing method of continuous fiber reinforced metal matrix composite. Chin J Mech Eng 2020; 33:31.
20. Tsai SW. Strength theories of filamentary structures fundamental aspects of fibre reinforced plastic composites. New York: Wiley-Interscience. 1968; 3–11.
21. Hashin Z, Rotem A. A fatigue failure criterion for fiber reinforced materials. J Compos Mater 1973;7:448–64.
22. Hashin Z. Failure criteria for unidirectional fiber composites. J Appl Mech 1980; 47(2): 329–34.
23. Hou JP, Petrinic N, Ruiz C, Hallett SR. Prediction of impact damage in composite plates. Compos Sci Technol 2000; 60(2): 228–73.
24. Puck A, Schürmann H. Failure analysis of FRP laminates by means of physically based phenomenological models. Compos Sci Technol 2002; 62: 1633–62.

25. Abaqus® 6.10 Analysis user’s manual. Dassault Systèmes; 2010.
26. Zheng JY, Shu XY, Wu YZ, Xu HJ, Lu QJ, Liao BB, Zhang BF. Investigation on the plastic deformation during the stamping of ellipsoidal heads for pressure vessels. Thin Wall Struct 2018; 127: 135–144.
27. Xia FK, Yu TX, Durandet Y, Ruan D. Triangular corrugated sandwich panels under longitudinal bending. Thin Wall Struct 2021; 169: 108359.

Figures

Figure 1

3D printing trajectories for CCF composites with (a) negative Poisson’s ratio or (b) high stiffness, and (c) an auxetic specimen subjected to a compression test.

Figure 2

(a) A front view of 3D-printed CCF composite structure with negative Poisson’s ratio and determination of 3D-printed CCF/PA and SCF/PA parts, (b) a bottom view and through-thickness distribution of 3D-printed CCF/PA and SCF/PA parts, and (c) meshwork of a CCF/PA composite with boundary conditions.

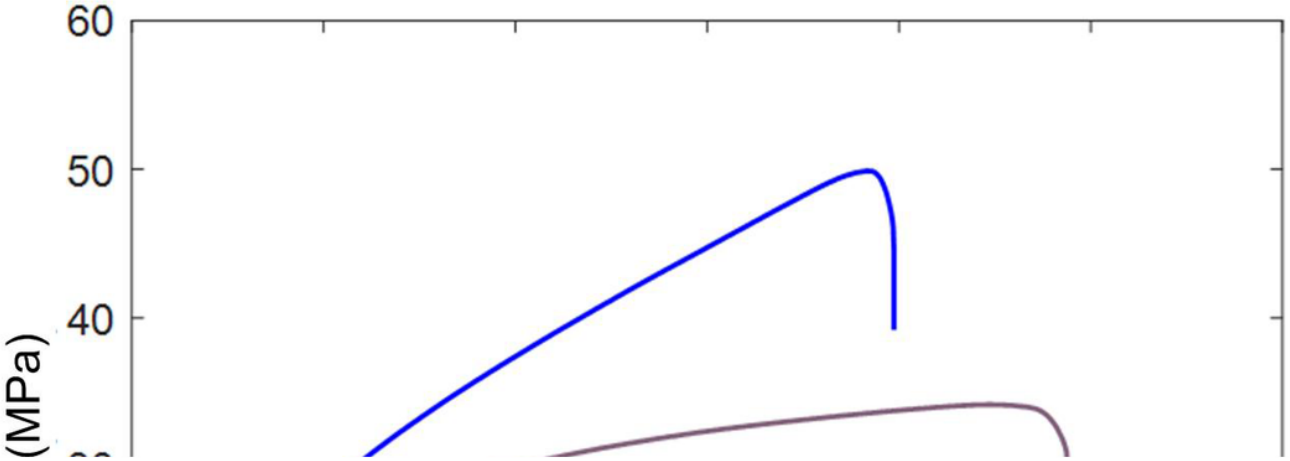

Figure 3

Experimental engineering and true stress-strain curves of 3D-printed SCF/PA specimens (deposited in ±45° configurations).

Figure 4

Comparison of force-displacement curves and DIC photographic analysis of horizontal strain ε_{xx} by experiments and von Mises stress by simulation at Point A of 4 mm for 3D-printed CCF/PA auxetic composites.

Figure 5

Failure mechanisms in terms of CCF/PA damage and SCF/PA deformation at displacement Point A of 4 mm for 3D-printed CCF/PA auxetic composite.

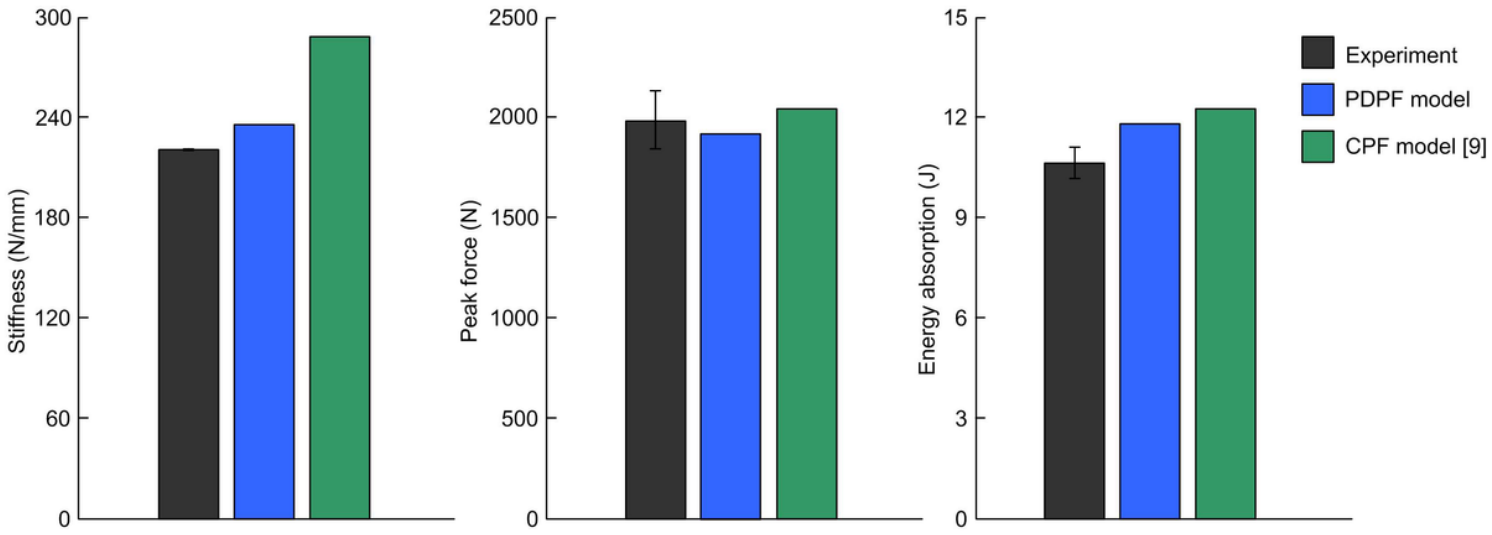

Figure 6

Mechanical performance and model effectiveness for the 3D-printed CCF/PA auxetic composite in terms of (a) stiffness, (b) peak force and (c) energy absorption.

Figure 7

Comparison of force-displacement curves and DIC photographic analysis of horizontal strain ε_{xx} by experiments and von Mises stress by simulation at Point A of 2 mm for 3D-printed CCF/PA high stiffness composites.

Figure 8

Failure mechanisms in terms of CCF/PA damage and SCF/PA deformation at displacement Point A of 2 mm for 3D-printed CCF/PA high stiffness composite.

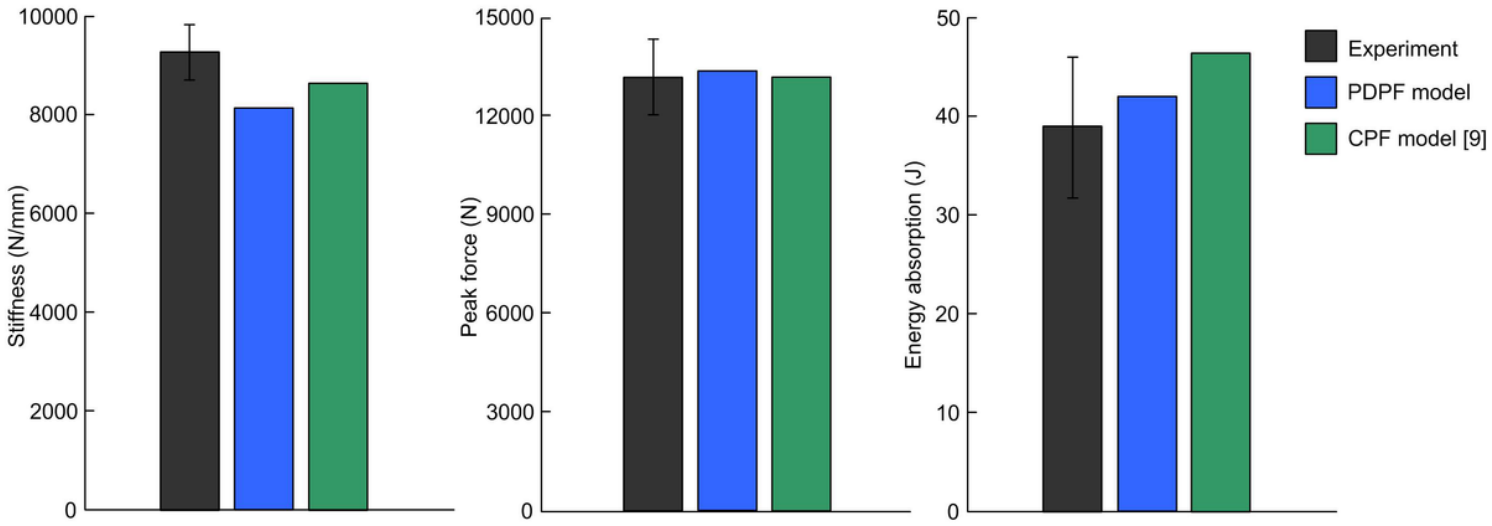

Figure 9

Mechanical performance and model effectiveness for the 3D-printed CCF/PA high stiffness composite in terms of (a) stiffness, (b) peak force and (c) energy absorption.

Supplementary Files

This is a list of supplementary files associated with this preprint. Click to download.

- Appendix.docx